Elastic scattering of ^{27}Al+^{27}Al at near barrier energies

A. Zerwekh, R. Liguori Neto, N. Added, J. C. Acquadro, N. Carlin, M. Frizzarini, and F. Malandrino
Instituto de Física, Universidade de São Paulo, C.P. 20516, São Paulo, 01498-970, Brazil

J. Lubian,* R. Cabezas, P. R. S. Gomes, R. M. Anjos, G. M. Santos, A. M. M. Maciel, C. Muri, and S. B. Moraes
Instituto de Física, Universidade Federal Fluminense, Av. Litoranea s/n, Gragoatá, Niterói, R.J., 24210-340, Brazil

G. Ramirez and C. Tenreiro
Departamento de Física, Facultad de Ciencias, Universidad de Chile, Casilla 653, Santiago, Chile

Elastic scattering angular distributions for the symmetric ^{27}Al+^{27}Al system were measured at bombarding energies from 50 to 70 MeV. The integrated inelastic cross section for the first two excited states was determined by the in-beam γ-ray spectroscopy method. The data were analyzed by the optical model and by coupled channel calculations. The spin-orbit couplings of the ground states of both nuclei are analyzed. [S0556-2813(98)02112-8]

I. INTRODUCTION

The elastic and inelastic scattering of asymmetric systems, at near barrier energies, have been investigated extensively in the last years. Very interesting results have come out from these studies, including the threshold anomaly of the optical potential at low energies and the coupling effects on the fusion process [1]. For two identical nuclei, the Coulomb scattering is described by the Mott distribution, which exhibits a pronounced interference pattern in the angular distribution. Near barrier scattering for such systems show fine structures and deviations from the Mott angular distributions, which are easier to be detected than those from the structureless angular distributions of the Rutherford scattering. Therefore, the scattering of identical particles is very sensitive to details of the nuclear potential and should allow the derivation, with high accuracy, of the optical model parameters. There are very few symmetric systems of identical sd-shell nuclei for which the elastic scattering have been measured [2–4]. All of them are for n-α nuclei. As the ^{27}Al is a nucleus with a ground-state spin equal to 5/2, the measurement of the scattering of the ^{27}Al+^{27}Al system allows also the investigation of the influence of the ground-state spin of the nuclei on the scattering and reaction processes.

In Sec. II of this paper the experimental methods and results are presented. In Sec. III, the elastic scattering of identical particles is described, and the optical model analysis of the elastic scattering data is discussed. In Sec. IV, the results of the coupled channel analysis of inelastic scattering are shown. Finally, in Sec. V, some conclusions are drawn.

II. EXPERIMENTAL DETAILS AND RESULTS

The experiments were performed at the 8UD Pelletron accelerator of the University of São Paulo. The beam intensity on the target was typically of the order of 10–50 nA. Experiments have been performed at seven bombarding energies from 53 to 70 MeV (the nominal Coulomb barrier is $E_{\text{Lab}} \cong 54$ MeV). There were targets with thickness of 15 and 50 μg/cm^2. A layer of 5 μg/cm^2 of ^{197}Au was deposited on the targets, for calibration and normalization purposes. The detection system was an array containing nine silicon surface barrier detectors. The angular separation between two adjacent detectors was 5°. In front of each detector there were collimators with diameters of 4 mm. The angle determination was made by reading on a goniometer with a precision of ±0.5°. A monitor was placed at 20° with the beam direction. The normalization was made by two different methods. In both, the scattering was supposed to be purely of the Coulomb type: at forward angles for the ^{27}Al target (Mott scattering) and for the ^{197}Au target (Rutherford scattering).

The angular distribution range of the data was taken from very forward angles up to $\theta_{\text{Lab}} = 70°$. The energy resolutions of the detectors were in the range from 300 keV [full width at half maximum (FWHM)], for forward angles and thin targets, to 1000 keV (FWHM) for backward angles and thick targets. Due to the kinematical broadening, the resolution was not good enough to separate the elastic and first inelastic (0.844 MeV) peaks of the ^{27}Al at backward angles. Furthermore, at backward angles, the elastic scattering was superposed with the recoil peaks of the ^{12}C and ^{16}O contamination. As a consequence of that, some asymmetries were noticed in the elastic angular distributions, with respect to $\theta_{\text{c.m.}} = 90°$. Therefore, in order to avoid these systematic errors, and using the fact that target and projectile are indistinguishable, only the data in the range up to $\theta_{\text{c.m.}} = 90°$ were used in the analysis.

Figure 1 shows a spectrum at $E_{\text{Lab}} = 55$ MeV, $\theta_{\text{Lab}} = 49°$. One can see the first two inelastic peaks with very small intensities and well resolved from the elastic peak.

The uncertainties in the elastic cross sections are due to the statistical errors and possible normalization errors. They were found to be smaller than 5%.

A further investigation of the integrated inelastic scattering cross section was performed by the in-beam γ-ray spectroscopy method. Two HP germanium detectors were placed
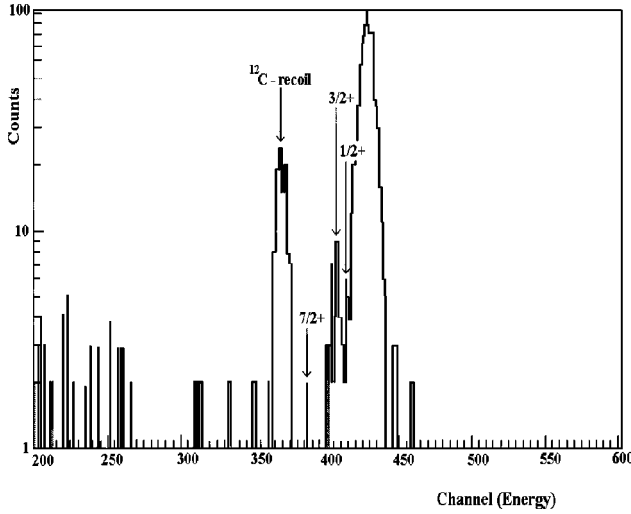
FIG. 1. Energy spectrum at $E_{lab}=55$ MeV and $\theta_{Lab}=49°$.

at $\pm 55°$ with the beam direction. The angular distributions of the γ rays follow the expression

$$W(\theta)=A_0+A_2 P_2(\cos\theta)+A_4 P_4(\cos\theta)+\cdots;\quad A_4\ll 1. \tag{1}$$

As $P_2(\cos 55°)=0$, it is possible to find the integrated cross section from $W(\theta=55°)$. The target had a thickness of $80\ \mu g/cm^2$ and was deposited on a Tantalum backing, thick enough to stop the beam. The energy resolution of the detectors was 2.2 keV (FWHM) at 1.33 MeV. Single and coincidence spectra were obtained for two bombarding energies: 55 and 61 MeV. The 844 and 1014 keV transitions, corresponding, respectively, to the first $(1/2^+)$ and second $(3/2^+)$ excited states of the ^{27}Al, were identified in the single spectra, but not in the coincidence ones. This confirms their identification as independent transitions to the ground state of the ^{27}Al. The integrated cross sections were, then, derived to be

for $E_{Lab}=55$ MeV, $\sigma_{1/2}^+=21.9\pm 1.2$ mb,

and $\sigma_{3/2}^+=21.7\pm 1.2$ mb;

for $E_{Lab}=61$ MeV, $\sigma_{1/2}^+=26.4\pm 1.4$ mb,

and $\sigma_{3/2}^+=26.4\pm 1.4$ mb.

III. ELASTIC SCATTERING ANALYSIS

For the scattering of identical nuclei, the wave function of relative motion must be antisymmetric with respect to exchange of the two nuclei. This is equivalent to the transformation $\theta\to\pi-\theta$. Therefore, we can write for the scattering amplitude

$$f_s(\theta)=f(\theta)+(-1)^s f(\pi-\theta), \tag{2}$$

where the amplitude $f(\theta)$ describes the scattering of distinguishable nuclei with identical properties and s is the total spin. The cross section could be obtained by incoherent superposition of the different possible s contributions according to their statistical weights [5]:
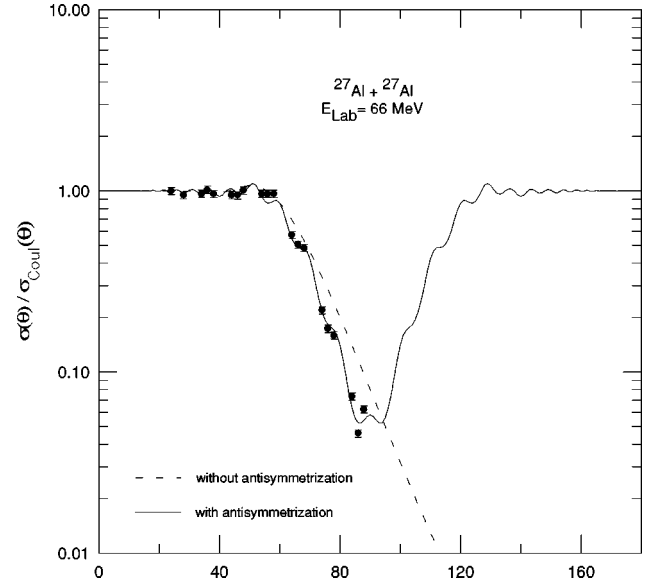

FIG. 2. Comparison of the calculation of the elastic angular distribution with and without effect of the antisymmetrization of the wave function, normalized at the cross section calculated with a pure Coulomb potential $[\sigma_{Coul}(\theta)]$.

$$\frac{d\sigma}{d\Omega}=\sum_{s=0}^{2I}\frac{2s+1}{(2I+1)^2}|f_s(\theta)|^2$$

$$=|f(\theta)|^2+|f(\pi-\theta)|^2+\frac{(-1)^{2I}}{2I+1}\{f(\theta)f^\star(\pi-\theta)$$

$$+f^\star(\theta)f(\pi-\theta)\}. \tag{3}$$

The elastic differential cross section of identical particles is usually normalized with respect to the Mott scattering formula [6]:

$$\left(\frac{d\sigma}{d\Omega}\right)_{Mott}=\frac{\eta^2}{4k^2}\left\{\csc^4\left(\frac{\theta}{2}\right)+\sec^4\left(\frac{\theta}{2}\right)+\frac{(-1)^{2I}}{2I+1}\right.$$

$$\left.\times 2\cos\left[\eta\ln\left(\tan^2\left(\frac{\theta}{2}\right)\right)\csc^2\left(\frac{\theta}{2}\right)\sec^2\left(\frac{\theta}{2}\right)\right]\right\}, \tag{4}$$

where η is the Coulomb parameter.

For the theoretical description of the angular distributions at each energy, the optical model was used, considering the optical potential in the form

$$V(r)=-V_0 f(r,R_{0v},a_v)-iW_{0V}f(r,R_{0w},a_v)+V_{Coul}, \tag{5}$$

where

$$f(r,R_{0i},a_i)=\frac{1}{1+\exp[(r-R_{0i})/a_i]};$$

and $R_{0i}=r_{0i}(A_p^{1/3}+A_t^{1/3});\quad i=v,w.$

V_0 and W_{0V} are the real and volume imaginary depth and r_{0i} and a_{0i} their radii and difusenesses. $f(r,R_{0i},a_{0i})$ is the form factor of Wood-Saxon and V_{Coul} is the Coulomb potential of

TABLE I. Sets of OMP's that equally well fit the experimental data, at different diffusenesses.

E_{Lab} (MeV)	53	55	57	60	63	66	70
			$a_v=a_w=0.72$ fm				
V_0 (MeV)	59.03	32.61	25.07	26.81	20.16	18.10	19.61
W_V (MeV)	2.15	2.39	4.21	5.06	5.07	5.07	5.08
W_S (MeV)	8.33	5.67	5.03	4.68	4.61	4.57	3.16
χ^2/N	3.03	2.27	3.00	1.34	3.69	4.71	2.05
			$a_v=a_w=0.67$ fm				
V_0 (MeV)	75.56	37.86	28.85	32.79	24.22	23.90	27.36
W_V (MeV)	6.62	7.07	8.21	10.78	10.93	11.09	11.31
W_S (MeV)	13.63	8.27	7.02	6.18	5.95	5.47	3.46
χ^2/N	3.25	2.31	2.91	1.39	5.13	3.27	1.58
			$a_v=a_w=0.62$ fm				
V_0 (MeV)	95.82	48.98	30.47	41.56	36.06	35.35	39.67
W_V (MeV)	8.59	12.48	12.93	13.0	13.51	14.91	14.51
W_S (MeV)	25.63	12.67	11.02	9.68	9.02	8.7	3.76
χ^2/N	3.07	2.37	2.87	1.46	6.00	2.40	1.74
			$a_v=a_w=0.57$ fm				
V_0 (MeV)	129.81	69.83	54.96	56.63	57.09	57.46	61.06
W_V (MeV)	16.94	21.63	23.01	23.21	23.86	24.37	24.39
W_S (MeV)	49.23	22.79	18.03	14.98	13.85	13.47	3.82
χ^2/N	3.12	2.47	3.11	1.52	6.87	2.08	2.26
			$a_v=a_w=0.52$ fm				
V_0 (MeV)	213.89	112.95	87.36	82.67	88.46	100.97	104.31
W_V (MeV)	22.06	36.75	38.17	42.39	42.97	43.63	44.39
W_S (MeV)	99.73	36.67	30.05	25.68	14.92	13.57	4.12
χ^2/N	3.11	2.60	2.98	1.71	4.55	1.88	3.89
			$a_v=a_w=0.47$ fm				
V_0 (MeV)	440.47	213.10	187.36	134.18	167.96	187.76	203.68
W_V (MeV)	36.42	43.39	60.72	65.99	71.29	82.06	82.39
W_S (MeV)	221.23	74.31	52.48	50.98	16.23	14.27	4.92
χ^2/N	3.28	2.75	2.95	1.66	4.02	1.78	3.45
			$a_v=a_w=0.42$ fm				
V_0 (MeV)	1179.37	490.74	360.55	367.57	363.70	388.76	459.21
W_V (MeV)	60.12	68.08	81.72	86.70	81.39	93.62	94.12
W_S (MeV)	568.23	167.27	124.44	89.31	21.23	14.97	4.71
χ^2/N	3.40	2.92	3.00	1.77	4.31	1.83	11.7

a uniform charged sphere with radius $R_C=1.5(A_p^{1/3}+A_t^{1/3})$. A_p and A_t are the projectile and target mass, respectively.

All the calculations were performed using the coupled-channel code ECIS [7]. This code, in its original version, does not take into account the projectile-target antisymmetrization for nonzero spins. Some modifications of the code were, therefore, implemented in order to calculate simultaneously the scattering amplitudes $f(\theta)$ and $f(\pi-\theta)$ [8]. Then, the angular distributions were computed using formulas (2) and (3). In Fig. 2 it is shown the elastic scattering differential cross sections for ^{27}Al+^{27}Al at 66 MeV for forward angles. The full line represents the elastic scattering cross section normalized by Rutherford cross section and the dotted one— normalized by Mott cross section (3). One can see that the effect of antisymmetrization on the angular distribution is notable even at forward angles (especially in the region of

nuclear-Coulomb interference).

The optical model calculations were performed by taking, as a starting set of the optical model parameters, the one obtained in [9] for the neighbor system ^{27}Al$+^{28}$Si, at laboratory energy of 70 MeV. As a first step, a χ^2-fit procedure was carried out, adjusting the radii and diffusenesses at 70 MeV, where the nuclear effects are more significant. These values were then fixed as $r_{0v}=1.19$ fm; $r_{0w}=1.11$ fm; $a_v=0.624$ fm; $a_w=0.655$ fm, and used for fitting of the angular distributions at lower energies. A second fit was performed by varying the depth of the real and volume imaginary potential, V_0 and W_{0V}. The results showed the need of the inclusion of a surface imaginary part, W_{0S}, of the derivative form

$$W_S(r) = -4iW_{0S}\frac{d}{dr}f(r,R_{0v},a_v) \qquad (6)$$

in order to adjust the angular region around 90°, where the nuclear interaction becomes stronger. In this formula, W_{0S} is the depth of the surface imaginary potential. Its radius and diffuseness were taken equal to the ones of the real potential considering that the collective effects manifest themselves in the nuclear surface. The presence of this surface imaginary potential indicates that some inelastic processes could play a role in this reaction.

In order to reduce the ambiguities of the optical potential, a "radius of sensitivity" [10,11] was searched, by fitting V_0, W_{0V}, and W_{0S} at different diffusenesses in the region of 0.42 fm up to 0.72 fm by step of 0.05 fm, and fixing the reduced radii, r_{0v} and r_{0w}, at previously found values. At this radius all the families to be found will be equivalent.

The set of optical model parameters (OMP) obtained by this procedure is shown in Table I. A notable sensibility can be observed of the real and imaginary depths to the diffuseness parameter for different families of OMP with roughly the same χ^2. The reason for this dependence is evident. To obtain the same value of the real and imaginary part of the potential at the radius of sensitivity one has to have deeper potential if their diffusenesses are smaller and vice versa. Another feature of the OMP sets of Table I is an increase of the volume imaginary part and a decrease of the surface one as the energy increases. This is in agreement with the prescriptions of the optical model. This behavior could be due to the opening of the low-lying inelastic channels.

In Figs. 3 and 4, the radial behavior is shown of the real and imaginary part of the potential, respectively, by taking the optimum χ^2 at different diffusenesses for all bombarding energies. The crossing radii for the real and the imaginary part of the optical potential were found in the region of 9–10 fm. They are listed in Table II for all bombarding energies. The energy averaged "radius of sensitivity" was found at 9.83 fm.

In Fig. 5, it is shown the energy dependence of the potential at this radius. The error bars represent the range of deviation of potential corresponding to distinct sets of parameters with different values of diffusenesses and roughly the same χ^2. The full line represents the results of the calculations using the dispersion relations [12]. It can be seen from this figure, a rather smooth energy dependence of the real and imaginary parts of the optical potential, except for the
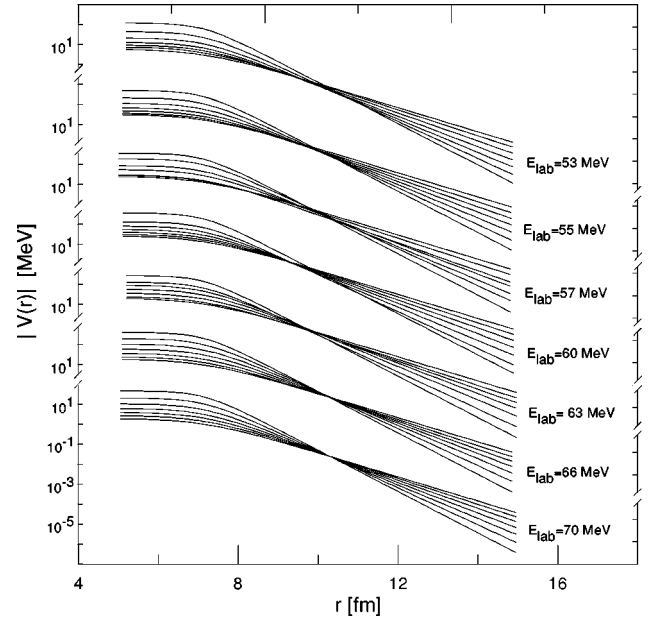

FIG. 3. Radial behavior of the real potential $V(r)$ for each measured energy, calculated by fitting the set of parameters corresponding to different diffusenesses in the range of 0.42–0.72 fm with approximately the same χ^2.

lower one, $E=53$ MeV, measured at sub-barrier Coulomb energy. This indicates that no optical potential anomaly is present near the Coulomb barrier for this system.

In Fig. 6, the results of the calculations using any of the equivalent sets of Table I (for each energy) are shown. The experimental error bars cannot be seen in the figure, because they are smaller than the points. One can see that the agreement of calculated cross sections with the experimental data is very good.

The influence of the spin-orbit interaction was tested by including, in the optical potential, a spin-orbit term of the
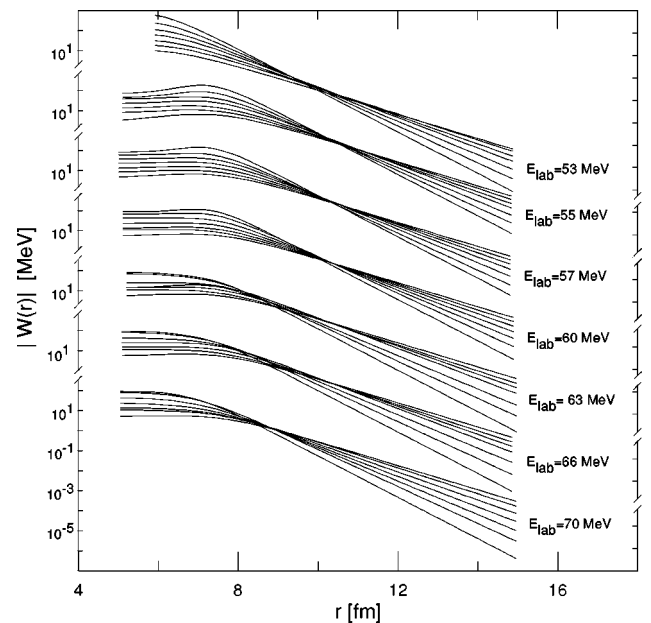

FIG. 4. The same as Fig. 3 for the imaginary potential $W_V(r)+W_d(r)$.

TABLE II. Radii of sensitivity R_{SV} (R_{SW}) for the real (imaginary) part of the optical potential at each bombarding energy.

E_{Lab} (MeV)	R_{SV} (fm)	R_{SW} (fm)
53	10.0	10.0
55	9.9	10.5
57	9.9	10.3
60	9.6	10.3
63	9.85	9.0
66	10.25	9.0
70	10.35	8.7
Mean value 9.83 fm		

Thomas form. In this way it was found that the depth of the spin-orbit potential at near barrier energies is an almost free parameter, i.e., keeping fixed the depth of the spin-orbit potential, one could fit the data varying the depth of the real and imaginary potentials by the same procedure explained above. On the other hand, when one includes the spin-orbit potential at higher energies (66 and 70 MeV) one could fit the experimental data only when the spin-orbit depth was very small (around 0.13 MeV). We conclude that the reason for this fact is that at near barrier energies, other processes, like the scattering of collective modes, play a most relevant role and the inclusion of the spin-orbit term is screened by the surface imaginary potential. At higher energies, the role of inelastic processes is less important and that is why the depth of the spin-orbit potential becomes relevant. Nevertheless, the small value of the spin-orbit potential depth obtained in the fit suggests that, even at higher energies, the spin-orbit interaction remains unimportant. Therefore, from
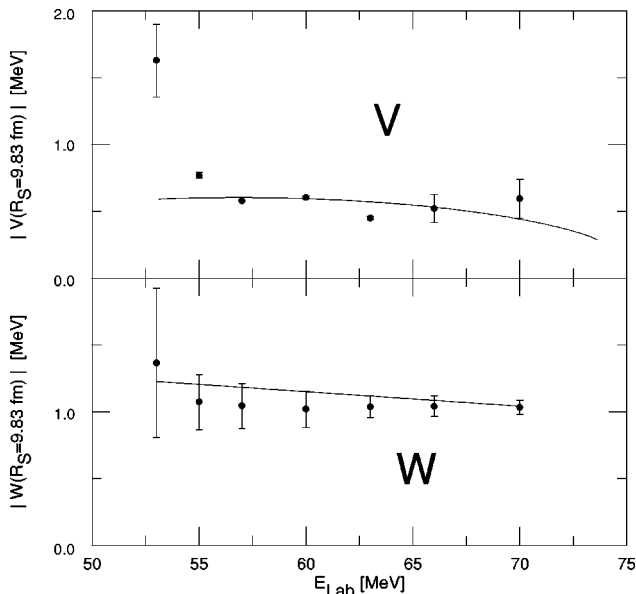

FIG. 5. Values of the real and imaginary part of the optical potential at "radius of sensitivity" equal to 9.83 fm. The full line corresponds to the dispersion relation calculations.
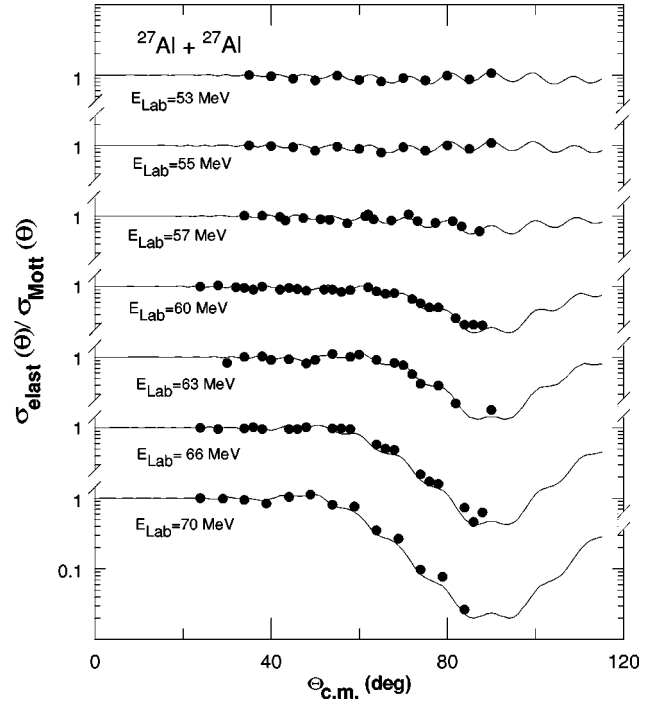

FIG. 6. Elastic scattering differential cross section for the system ^{27}Al+^{27}Al at different bombarding energies. The experimental error bars are smaller than the points. The full line corresponds to the optical model calculation using one of the sets of Table I.

this analysis we could state that the spin-orbit interaction does not play a significant role in the description of the elastic scattering in this system.

IV. INELASTIC SCATTERING COUPLING

In order to describe the inelastic cross section, coupled-channel calculations were performed considering a coupling scheme of three levels: $5/2^+(0.0\text{ MeV})$, $1/2^+(0.84\text{ MeV})$, and $3/2^+(1.01\text{ MeV})$. The excitations of the two low-lying excited states were determined by the off-diagonal matrix elements that connect these states to the ground state and these states between themselves, and the diagonal matrix elements, which give rise to the reorientation effects. The electric part of these matrix elements is known from the measured lifetime and quadrupole moments of these states [13]. The used values are listed in Table III. The excitation of the projectile was considered in the same way as the target excitation. The ^{27}Al is a single-hole nucleus where the unpaired particle is a proton in the $1d_{5/2}$ subshell. It is located in a transitional region between the prolate nucleus ^{26}Mg and

TABLE III. Summary of reduced matrix elements used in coupled-channel calculation taken from Ref. [13].

	$\langle I'||E2||I\rangle$ (in e b)		
	$I=5/2$	$I=1/2$	$I=3/2$
$I'=5/2$	0.198	-0.0883	0.125
$I'=1/2$	-0.0883	0	0 ± 0.1
$I'=3/2$	-0.125	0 ± 0.1	0 ± 0.12

TABLE IV. Experimental inelastic integral cross section for the excited states $1/2^+$(0.884 MeV) and $3/2^+$(1.014 MeV), and calculated cross section using the coupled-channel formalism.

E_{Lab} (MeV)	$\sigma_{1/2}^+$ (mb)	$\sigma_{3/2}^+$ (mb)	$\sigma_{reaction}$ (mb)
55	Exp 21.9±1.2	Exp 21.7±1.2	499
	Theor 4.4	Theor 23.02	
61	Exp 26.4±1.4	Exp 26.4±1.4	746
	Theor 13.6	Theor 22.6	

the oblate ^{28}Si [13,14]. Its measured quadrupole moment [15] and the $B(E2)$ values [16–18] are evidences of a large static deformation. The models used for its description indicate a deformed oblate shape. The potential deformation that determines the nuclear part of the matrix elements, in terms of the rotational model, were taken from [19]: $\beta_2 = 0.37$ for $1/2^+$ state and $\beta_2 = 0.35$ for $3/2^+$ state. The results of calculations and their comparison with the experiment are shown in Table IV. It can be seen that the derived inelastic scattering cross sections agree with the data for the $3/2^+$ state, but are lower than those for the $1/2^+$ state. For this system, coupled-channel calculations including these two excited states do not give significant improvement in the fit of the elastic angular distribution, when compared with the optical model calculations.

V. SUMMARY

In this paper we presented original elastic and inelastic scattering data on odd identical nuclei, for the ^{27}Al$+^{27}$Al system at sub- and near barrier energies. The present results show a rather smooth energy dependence of the optical potential at near barrier energies and suggest a small influence of the coupling of the considered states on the elastic scattering angular distributions. It would be interesting to study the influence of these collective effects on the fusion cross sections in the vicinity of the Coulomb barrier. In order to do that, measurements on the fusion excitation function and inelastic scattering cross sections near the barrier will be carried out. The influence of the spin-orbit interaction was found not to be important in the description of the elastic scattering process of this system.

[1] *Heavy-Ion Fusion: Exploring the Variety of Nuclear Properties*, edited by A. M. Stefanini, G. Nebbia, S. Lunardi, G. Montagnoli, and A. Vitturi (World Scientific, Singapore, 1994).

[2] H. Emlyng *et al.*, Nucl. Phys. **A239**, 172 (1975).

[3] B. Bilwes, R. Bilwes, L. Stuttge, F. Ballester, J. Diaz, J. L. Ferrero, C. Roldan, and F. Sanchez, Nucl. Phys. **A473**, 353 (1987).

[4] A. Thiel, W. Greiner, and W. Scheid, Phys. Rev. C **29**, 864 (1984).

[5] C. J. Joachain, *Quantum Collision Theory* (Elsevier, New York, 1975), p. 160.

[6] N. F. Mott, Proc. R. Soc. London, Ser. A **126**, 259 (1930).

[7] J. Raynal (unpublished).

[8] R. Cabezas and J. Lubian (private communication).

[9] S. K. Charagi, S. K. Gupta, M. G. Betigeri, C. V. Fernandes, and Kuldeep, Phys. Rev. C **48**, 1152 (1993).

[10] C. Muri, R. M. Anjos, R. Cabezas, P. R. S. Gomes, S. B. Moraes, A. M. M. Maciel, G. M. Santos, J. Lubian, M. M. Sant'Anna, C. Tenreiro, R. Ligouri-Neto, J. C. Acquadro, and P. A. B. Freitas, Eur. Phys. J. A **1**, 143 (1998).

[11] M. E. Brandan, J. R. Alfaro, A. Menchaca-Rocha, J. Gomez del Campo, G. R. Satchler, P. H. Stelson, H. T. Kim, and D. Shapira, Phys. Rev. C **48**, 1147 (1993).

[12] G. R. Satchler, Phys. Rep. **199**, 147 (1991).

[13] D. Schwalm, E. K. Warburton, and J. W. Olness, Nucl. Phys. **A293**, 425 (1977).

[14] C. Van Der Lenn, D. M. Sheppard, and P. M. Endt, Nucl. Phys. **A100**, 316 (1967).

[15] D. Dehnhard, Phys. Lett. **38B**, 389 (1972).

[16] R. Weber, B. Jeckelmann, J. Kern, U. Kiebele, B. Aas, W. Beer, I. Beltrami, K. Bos, G. De Chambrier, P. F. A. Goudsmit, H. J. Leisi, W. Ruckstuhl, G. Strassner, and A. Vacchi, Nucl. Phys. **A377**, 361 (1982).

[17] V. H. Thankappan, Phys. Rev. **141**, 957 (1967).

[18] D. Evers, J. Hertel, T. W. Retz-Schmidt, and S. J. Skorka, Nucl. Phys. **A91**, 472 (1967).

[19] P. M. Endt, At. Data Nucl. Data Tables **23**, 3 (1979).